Talanta 101 (2012) 192–197

Contents lists available at SciVerse ScienceDirect

Talanta

journal homepage: www.elsevier.com/locate/talanta

Fluorescence resonance energy transfer quenching at the surface of graphene quantum dots for ultrasensitive detection of TNT

Lishuang Fan [a], Yuwei Hu [a], Xiao Wang [b], Linlin Zhang [b], Fenghua Li [a], Dongxue Han [a], Zhenggang Li [a,*], Qixian Zhang [a], Zhenxin Wang [a,*], Li Niu [a,c]

[a] State Key Laboratory of Electroanalytical Chemistry, c/o Engineering Laboratory for Modern Analytical Techniques, Changchun Institute of Applied Chemistry, Chinese Academy of Sciences, Changchun 130022, P.R. China
[b] Jilin Product Quality Supervision Test Institute, Changchun 130022, P.R. China
[c] Changzhou Institute of Energy Storage Materials and Devices, Changzhou 213001, P.R. China

ARTICLE INFO

Article history:
Received 14 June 2012
Received in revised form
27 August 2012
Accepted 28 August 2012
Available online 3 September 2012

Keywords:
Graphene
Graphene quantum dots
Fluorescence
Fluorescence resonance energy transfer
TNT

ABSTRACT

This paper for the first time reports a chemical method to prepare graphene quantum dots (GQDs) from GO. Water soluble and surface unmodified GQDs, serving as a novel, effective and simple fluorescent sensing platform for ultrasensitive detection of 2,4,6-trinitrotoluene (TNT) in solution by fluorescence resonance energy transfer (FRET) quenching. The fluorescent GQDs can specifically bind TNT species by the π–π stacking interaction between GQDs and aromatic rings. The resultant TNT bound at the GQDs surface can strongly suppress the fluorescence emission by the FRET from GQDs donor to the irradiative TNT acceptor through intermolecular polar–polar interactions at spatial proximity. The unmodified GQDs can sensitively detect down to ~0.495 ppm (2.2 μM) TNT with the use of only 1 mL of GQDs solution. The simple FRET-based GQDs reported here exhibit high and stable fluorescence. Eliminating further treatment or modification, this method simplifies and shortens the experimental process. It possesses good assembly flexibility and can thus find many applications in the detection of ultratrace analytes.

1. Introduction

Explosives play an important role in military and aerospace infrastructure,in some industrial fields, and in modern society, due to their effects on the environment and human health as well as global security concerns [1,2]. Selective and sensitive detection quantification of nitroaromatic explosives, such as TNT, have attracted much attention in recent years [3–5]. In the past decades, a number of new analytical methods, for example fluorescence, field effect transition, and surface plasmon resonance, have been developed for detection of TNT [6–8]. In particular, fluorescence is considered as one of the most promising approaches for explosives sensing because of its inherent sensitivity and high selectivity [9–11].

Quantum dots (QDs), or colloidal semiconductor nanocrystals, have been the center of much attention in the past few years [12–15]. Unlike organic fluorescent dyes, these QDs, which show a brand new class of fluorescent nanoprobes, are advantageous dyes because of their tunable emission color, unique optical and electronic properties, high quantum yield, and long-term photostability. Moreover, emission of QDs is narrow, symmetric, and non-interfering with regard to the excitation and emission wavelength [16,17]. Due to their unique properties, QDs have found increased uses in a variety of practical biological applications [18–22]. As novel luminescent probes, QDs have also attracted considerable attention in the development of sensitive and selective fluorescence sensors in recent years [23,24].

Graphene, a single layer of carbon atoms densely packed in a honeycomb two-dimensional (2D) lattice, has been demonstrated to have unique electronic, thermal, photonic, and mechanical properties, which make it very attractive in physics, chemistry, and material science [25,26].It has been both theoretically predicted and experimentally proven that the morphology of graphene sheets, including size, shape and thickness can effectively determine their properties [27–29]. Theoretical and experimental studies of graphene have indicated that its bandgap and optical properties can be manipulated by reducing its size to a nanolevel, where it is also called graphene quantum dots (GQDs) [30,31]. GQDs possess strong quantum confinement and edge effects, which make them excellent materials for the construction of nanoscale optical, bioimaging, and electronic devices [32,33].

To fabricate GQDs, some papers concerning fluorescent graphene have been published and applied [27–29,32–36]. Due to stable photoluminescence, low toxicity, excellent solubility, and

* Corresponding authors. Fax: +86 431 8526 2800.
E-mail addresses: leegon@ciac.jl.cn (Z. Li), wangzx@ciac.jl.cn (Z. Wang).

0039-9140/$ - see front matter © 2012 Elsevier B.V. All rights reserved.
http://dx.doi.org/10.1016/j.talanta.2012.08.048

biocompatibility, their usage has been expanded to application in optoelectronics and for biological probes [22,36–39]. In addition to the properties mentioned above, GQDs have some advantages in detection of TNT compared with other QDs. Firstly, GQDs form two-dimensional and one atom thick planar sheets of sp^2-bonded carbon atoms. The restored π-network provides a good substrate for anchoring π-conjugated molecules through π–π stacking interaction, which is beneficial in detecting TNT and very efficient for fluorescent quenching. Second, GQDs have an incomparable advantage over other QDs as they do not need treatment or modification before they are used for direct detection, which simplifys and shortens the experimental process.

Herein, we report that fluorescence of GQDs could be quenched by nitroaromatic analytes based on FRET, which might provide a new pathway for the detection of nitroaromatic explosives and their related compounds.

2. Experimental details

2.1. Materials

Graphite powders (320 mesh) as spectroscopically pure reagents were obtained from Shanghai Chemicals, China. 2,4,6-trinitrotoluene (TNT) was obtained from Sigma-Aldrich. 2,6-dinitrotoluene (2,6-DNT), and 4-mononitrotoluene (4-NT) were obtained from Alfa Aesar. Sodium borohydride ($NaBH_4$, 96%) was purchased from Beijing Yili Chemicals, China. Unless otherwise stated, other reagents were of analytical grade and were used as received. All aqueous solutions were prepared with ultra-pure water (>18 MΩ) from a Milli-Q plus system (Millipore).

2.2. Apparatus

Fourier transform infrared spectroscopy (FTIR) was carried out with a Bruker Tensor 27 Spectrometer (4 cm^{-1}). Transmission electron microscopy (TEM) images were taken with a TECNAI G2 high-resolution transmission electron microscope. Atomic force microscope (AFM) images were obtained with a microscope (Seiko Instruments Industry Co., Tokyo, Japan). Raman analysis was carried out with a J-Y T64000 Raman spectrometer with 514.5 nm wavelength incident laser light. XPS measurements were conducted with a VG ESCALAB MKII spectrometer. Zeta potential was recorded on a Nano-ZS instrument. UV–vis absorption spectra were recorded using a Hitachi U-3900 spectrophotometer. Fluorescence emission spectra were recorded using a Hitachi F-4600 fluorescence spectrophotometer with an excitation wavelength of 350 nm. Excitation and emission slit widths were both 10 nm. Photoluminescence decay was measured on a Photon Technology International (PTI) Time Master fluorescence lifetime spectrometer equipped with a GL-302 dye laser pumped by a PTI GL-3300 nitrogen laser and a GL-303 frequency doubler.

2.3. Preparation of graphene quantum dots

Graphene oxide (GO) was synthesized using the modified Hummers method [40].Graphene sheets (GS) were obtained by reduction of GO sheets with $NaBH_4$ at 85 °C for 12 h [41]. GS (150 mg) were oxidized in HNO_3 (30 mL) for 20 h at 90 °C. After cooling to room temperature, the oxide GS (OGS) was reduced with $NaBH_4$ at 85 °C for 12 h after the pH was tuned to 9 with NaOH. Then the mixture was further dialyzed in a dialysis bag (retained molecular weight: 3500 Da).

2.4. Fluorescence detection of TNT

Various concentrations of TNT were added to solution of GQDs (1 mL). The solution was mixed thoroughly at room temperature for 30 s. The fluorescence quenching spectra was then recorded (excitation 350 nm; emission 446 nm). The interfering effects of other metal ions were investigated individually.

3. Results and discussion

3.1. Morphology characterization of GQDs

The chemical reduction processes lead to the partial removal of an oxygen-containing group and repair of the aromatic structures, which promotes the stability of GQDs in aqueous solutions and recovery of sp^2 hybridization [42].The GQDs were prepared from GS by oxidization treatment with HNO_3, and then by reduction treatment with $NaBH_4$. The prepared GQDs possess strong fluorescence with PL quantum yields of 5.5% (see ESI† for details and Table S1). Some conventional measurement methods were used to describe the size, shape, and structure of GQDs. Typical TEM shows that diameters of 1 μm of GS (Fig. 1a) became slightly smaller at 50 nm of OGS (Fig. 1b) and 6 nm (average diameter) of GQDs (Fig. 1c) after chemical oxidization and reduction. The AFM images in Fig. 1d show the topographic of GQDs, wherein the heights are mostly between 1 and 3 nm, similar to those observed in functionalized graphene nanoribbons with 1–3 layers [43].

3.2. Spectral characterization of GQDs

The functional groups on the OGS surface and the GQDs surface were confirmed by using FTIR (Fig. 2a). The spectrum of OGS illustrates the presence of C–OH (υ_{C-OH} at 1415 cm^{-1}), C═O ($\upsilon_{C=O}$ at 1733 cm^{-1} in carboxylic acid and carbonyl moieties) and C–O–C (υ_{C-O-C} at 1255 cm^{-1}). Compared with OGS, the spectrum of GQDs is essentially featureless except for the C═C

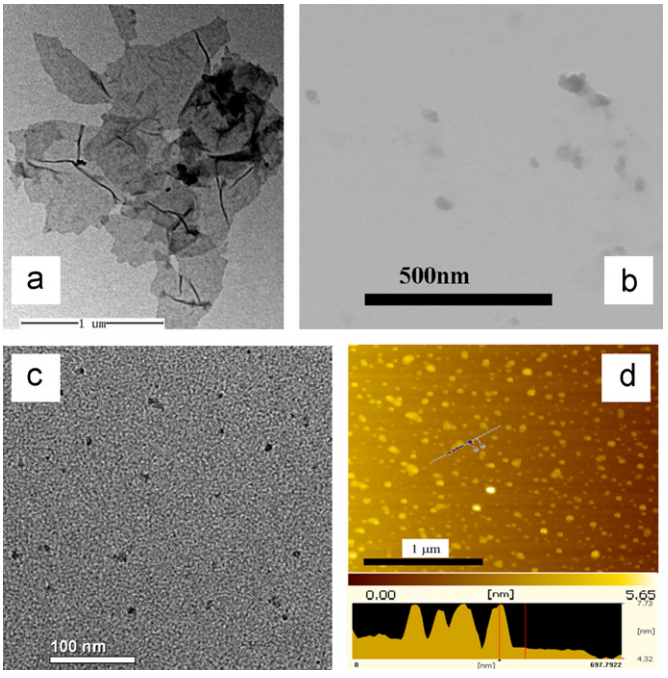

Fig. 1. (a, b, c) TEM image of the GO, OGS, and GQDs. (d) AFM image of the dots deposited on freshly cleaved mica substrates.

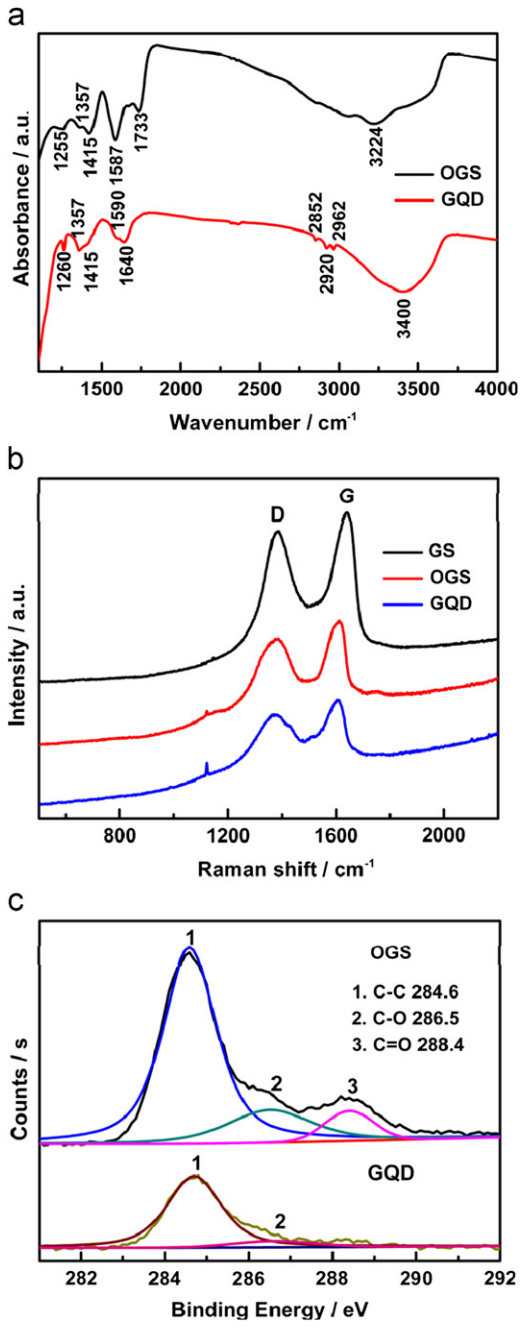

Fig. 2. (a,c) FTIR and XPS C 1 s spectra of the OGS and GQDs. (b) Raman spectrum of GS, OGS, and GQDs.

peak at 1640 cm^{-1} and a sharper O–H peak at 3400 cm^{-1}. The adsorption bands of oxygen functionalities disappear (C═O), which confirm that OGS can be achieved by the chemical reduction process. Raman spectroscopy is another powerful and widely used technique to characterize the structure and some properties of GS, OGS and GQDs display two prominent peaks D band (~1380 cm^{-1}) and G band (~1610 cm^{-1}). The Raman spectrum of corresponding to the well-documented D and G bands, respectively, was shown in Fig. 2b. The I_D/I_G ratio of the GQDs (0.912) was found to be decreased compared to that of initial graphene (0.929) and OGS (0.917), revealing a substantial increase in the content of the sp^2-bonded carbon atoms and the oxidized molecular defect domains from GQDs [44,45]. The results, combined with FTIR, provide further confirmations for the formation of GQDs by the defect by cutting GS. In other words, the directions of epoxy chains formed in GS are cut leading to formation of graphene quantum dots.

The curve fit of C1s spectra of OGS and GQDs is shown in Fig. 2c. The XPS spectrum of OGS indicates the presence of three main types of carbon bonds: C–C (284.6 eV), C–O (286.5 eV), and C═O (288.4 eV). After its chemical reduction, the peaks associated with C–C (284.6 eV) become predominant, whereas the peaks related to the oxidized carbon species are greatly weakened. These results further indicate that OGS has been well deoxygenated to form GQDs.

The UV–vis absorption spectra of GQDs are shown in Fig. 3a. The spectra of GQDs show a new absorption peak at 300 nm. On excitation of the absorption band of 350 nm, the PL spectrum shows a strong peak at 446 nm as well as a shoulder peak at 570 nm with a Stokes shift of 96 nm (0.764 eV). Different GQDs exhibit multicolored luminescence and strong fluorescence response relative to OGS and GO (Fig. S1). The GQDs also exhibit excitation dependent PL behavior. When the excitation wavelength is from 300 nm to 540 nm, the PL peak shifts to a longer wavelength (from 446 nm to 575 nm) and its intensity decreases rapidly with the strongest peak excited at the absorption band (Fig. 3b). Two electronic transitions of 353 nm (3.52 eV) and 267 nm (4.65 eV) observed in the photoluminescence spectrum of GQDs can be regarded as transitions from σ and π orbitals, viz., the highest occupied molecular orbital (HOMO) to the lowest unoccupied molecular orbital (LUMO) (Fig. S2) [32,46]. The PL in graphene depends on the chemical nature of the graphene edges, which is explained in detail by Radovic et al. [46]. The GQDs show very good fluorescence stability at different pH, ionic strength, hold and irradiation time (Fig. S3). The change of GQDs fluorescence intensity with pH variation was only observed when the titration of the sensing solution was performed with strong acid or base. The fluorescence intensity changes slightly with different pH (Fig. S3a). This observation may be due to a stability effect on the dots surface charge status by the buffer solution. Results have been reported that the aromatic hydroxyl group of GO would be deprotonated, which results in a drop of fluorescence intensity [47]. Because the GQDs surface possesses bits of carboxyl group, the pH effect on it is weak. Fig. S3b shows the effect of Cl^- on GQDs fluorescence and a weak quenching of the fluorescence intensity is observed. Zeta potential of GQDs is −34 mV by representing sufficient mutual repulsion to ensure the stability of a dispersive solution. The fluorescence intensity does not change at milimolar level chloridion, which is electron drawing group. With chloridion concentration increasing, the fluorescence decreases due to the exclusion of intermolecular leading to the change of GQDs surface dielectric properties of the surrounding medium. Nevertheless, the PL of GQDs is sensitive to the species of the solvent. This solvent effect could be induced by a lone electron pair, which changes the electron state of GQDs and can affect fluorescence (Fig. S4). These data suggest that GQDs exhibit strong PL stability.

3.3. FRET-based GQDs sensors for TNT detection mechanism

Because the GQDs show good stability, water solubility, and multicolor, they can be directly used for detection of TNT. Fig. 4a shows a schematic drawing of a GQDs sensor for TNT detection. The GQD surface is not treated or passivated. The primary π-network at the surface of the GQDs plays the role of a recognition receptor of TNT molecules by the strong specific π–π stacking interaction and electrostatic adhesion. A TNT analyte is thus attached to the surface of GQDs in the form of a TNT–GQDs complex. Analyte binding will lead to the quenching of GQDs fluorescence through two possible pathways: the FRET and the common charge transfer from GQDs to TNT. Part 1 of Fig. 4b

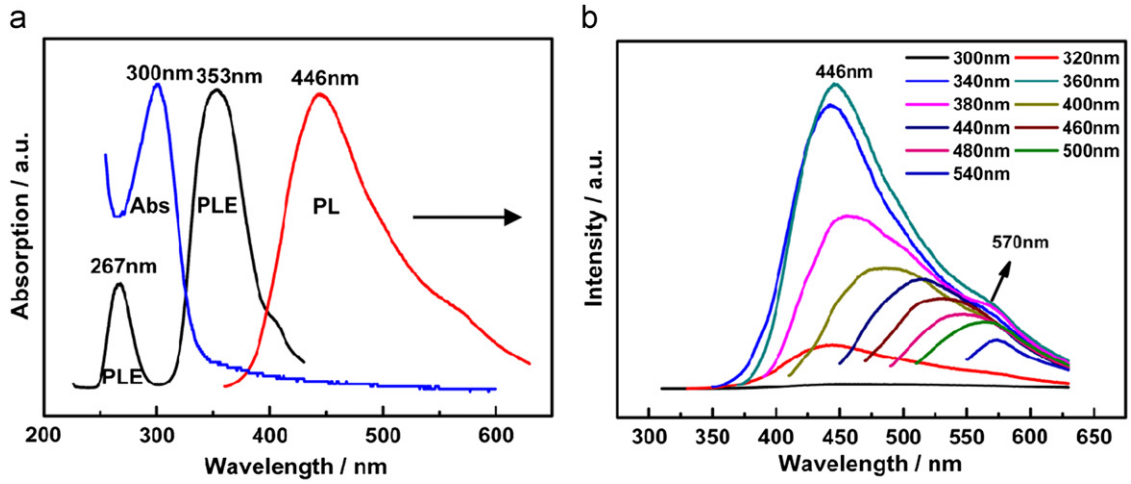

Fig. 3. (a) UV–vis absorption (Abs, blue) and PLE (black), PL (at 350 nm excitation) spectra of the GQDs dispersed in water. (b) PL spectra of the GQDs at different excitation wavelengths (For interpretation of the references to color in this figure caption, the reader is referred to the web version of this article.).

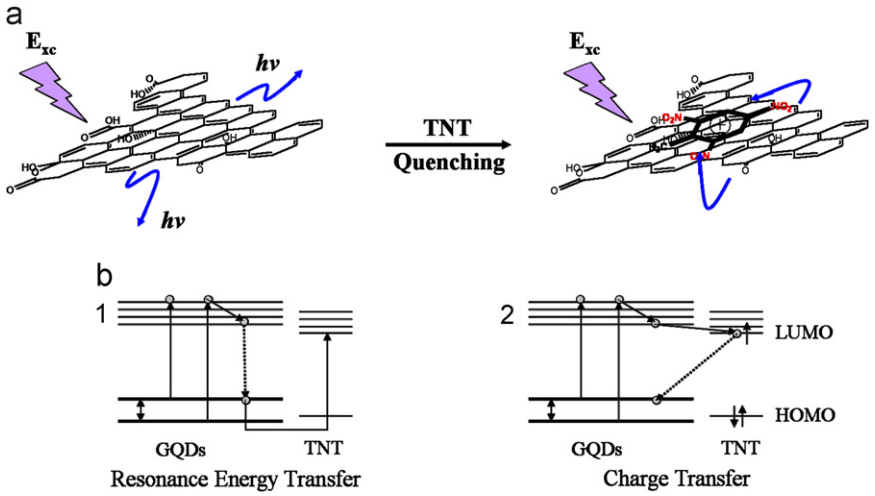

Fig. 4. (a) Schematic of the FRET-based GQDs sensor for detection of TNT. (b) Quenching mechanism through (1) resonance energy transfer from the GQDs donor to TNT acceptor and (2) charge transfer from the excited GQDs to TNT.

illustrates the quenching mechanism of GQDs fluorescence through FRET from the GQDs donor to the TNT acceptor. When the excited-state electron of the GQDs donor returns to the ground state, the ground state electrons of the TNT transit to the excited state. Due to the polar–polar resonance of the donor and acceptor, the coupling transitions result in highly efficient quenching of GQDs fluorescence. FRET is a predominant quenching process in the case of the TNT and greatly amplifies the fluorescence quenching response to the TNT analyte. On the other hand, it should be noted that the fluorescence of GQDs and TNT molecules may also be quenched by the charge transfer mechanism, as illustrated in part 2 of Fig. 4b. The excited-state electrons transfer to the LUMO of TNT when GQDs meet TNT. Then, the electrons return to the ground state with a radiationless transition caused by the quenching of fluorescence. The mechanism is expounded by the UV–vis. Fig. S5 shows that the UV–vis absorption peak has a blue shift when TNT is added. The lone pair electrons and big π–π conjugated system of GQDs–TNT composite charge transfer interaction and partly inhibitory action lead to the absorption peak moving to a shorter wave (blue shift). This indicates common charge transfer fluorescence quenching with TNT at the surface of GQDs. Furthermore, the excited state lifetime of the GQDs before and after addition of TNT was also compared (0.70 ns, 74.4% for free GQDs and 2.11 ns, 50% for the GQDs–TNT complex. See Fig. S6 and Table S2). We conjecture that the significant ultrafast process to charge transfer from the excited GQDs to the GQDs–TNT complexes results in fluorescence quenching of GQDs [48,49].

3.4. Determination of TNT and other system nitro-compound concentration

The FRET quenching of GQDs is applicable in detection of TNT analytes. The response to quenching of various concentration was analyzed using the Stern–Volmer equation [50]: $I_0/I=1+k_q\tau_0[Q]=1+K_{SV}[Q]$ where I_0 and I are the fluorescence intensities at 350 nm in the absence and presence of TNT, respectively, k_q is the bimolecular quenching constant, τ_0 is the lifetime of the fluorophore in the absence of quencher, K_{SV} is the Stern–Volmer fluorescence quenching constant, which is a measurement of the efficiency of quenching by quencher and [Q] is the quencher concentration. Linear Stern–Volmer relationships are observed for TNT in the ppm range (Fig. 5a). Fig. 5b shows the Stern–Volmer plots, I_0/I versus [TNT]. The resulted plots exhibited a good linear relationship in the range of 0.495–181.58 ppm ($R=0.997$). K_{SV}, calculated by linear regression of the plots, was $8\times10^3\ M^{-1}$. From the equation we know $K_{SV}=k_q\tau_0$. For GQDs–TNT, τ_0 is known to be 2.11 ns, thus $k_q=3.79\times10^{12}\ M^{-1}\ s^{-1}$. Since the

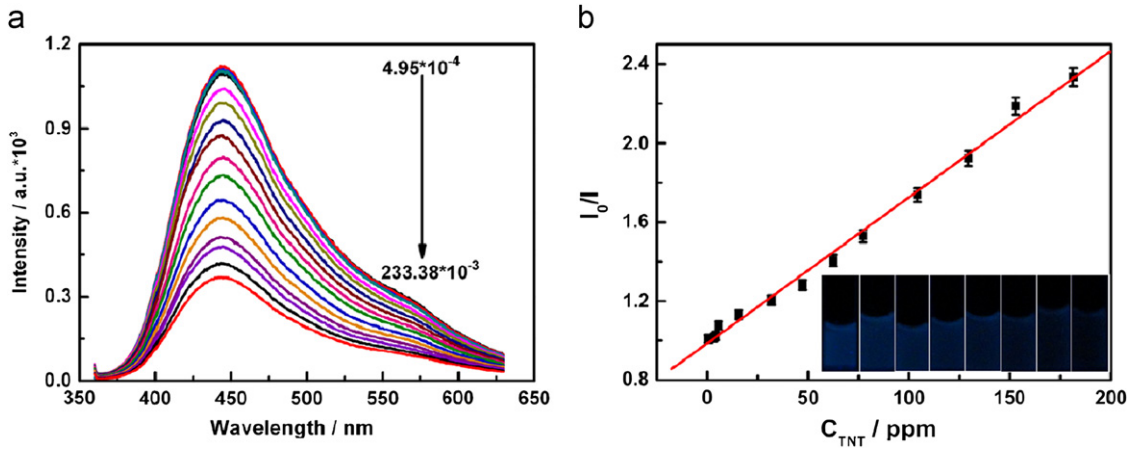

Fig. 5. (a) Emission spectra of GQDs in the presence of TNT (from 4.95×10^{-4} to 233.38×10^{-3} g/L). (b) Fluorescence intensity response of GQDs to different TNT concentration. Inset of visible fluorescence response of the GQDs in the different concentration of TNT.

maximum value of k_q for a diffusion controlled quenching process is about $10^{10}\,M^{-1}\,s^{-1}$, the higher value (over 380-fold) obtained here suggested that the quenching of GQDs fluorescence occurred by a specific interaction between GQDs and TNT. This also implied that the dominating quenching mechanism was static of FRET (formation of a complex). We further tested the quenching response to DNT and NT, which are structural analogues of TNT. As showed in Fig. S7, the quenching constants of GQDs with TNT are much larger than those with DNT and NT, respectively. These are again consistent with our expectation that the highest fluorescence quenching of GQDs with TNT is closely related to the formation of GQDs–TNT complexes at the surface of GQDs. It is well-known that DNT and NT are much weaker electronic acceptors than TNT molecules. All above results further confirm the highest fluorescence sensitivity and chemical selectivity for TNT analyte, due to the formation of the GQDs–TNT complexes and the highly efficient FRET-based quenching.

The GQDs detection of TNT reveals a high K_{SV} ($8\times10^3\,M^{-1}$), wide detection range (4.95×10^{-4}–1.82×10^{-1} g/L) and low detection limit (4.95×10^{-4} g/L) to dinitrotoluene and mononitrotoluene. Furthermore, the GQDs show better anti-interference for organic species (Table S3 and Fig. S8) and stable emission in the presence of O_2 [30].

4. Conclusions

In this work, we have developed a chemical method to prepare GQDs from GO, and the water soluble and multicolored fluorescent GQDs are adopted for the ultratrace TNT detection based on FRET for the first time. A Stern–Volmer fluorescence quenching constant with $8000\,M^{-1}$ in the linear range from 4.95×10^{-4} to 1.82×10^{-1} g/L of TNT and the attenuation of fluorescence intensity can clearly be detected down to 0.495 ppm (2.2 μM) in solution was obtained. Moreover, a large difference in quenching efficiency was observed for different types of nitroaromatic analytes, which is dependent on their electron-accepting ability. Compared to other QDs, GQDs displayed high stability and broad excitation in solution, and unmodified GQDs simplify and shorten the experimental process to detect TNT. Meanwhile, unique spectral properties of GQDs should eventually allow for the simultaneous FRET-based monitoring of multiple environmental contaminants using a single well of a microtiter plate or a flow cell. The requirements for future sensors will consider the multiplex format for multicolored GQDs-based sensors.

Acknowledgment

The authors are most grateful to the NSFC (Nos. 21175130 and 21105096), Department of Science and Technology of Jilin Province (No. 201215091), and Department of Science and Technology of Changzhou City (No. CJ20110016) for their financial support.

Appendix A. Supporting information

Supplementary data associated with this article can be found in the online version at http://dx.doi.org/10.1016/j.talanta.2012.08.048.

References

[1] E. D'Amico, Chem. Week 164 (2002) 25.
[2] S.T. Makrinos, Sea Technol. 45 (2004) 33.
[3] D.T.A. McQuade, E. Pullen, T.M. Swager, Chem. Rev. 100 (2000) 2537.
[4] A. Rose, Z.G. Zhu, C.F. Madigan, T.M. Swager, V. Bulović, Nature 434 (2005) 876.
[5] Q. Zhou, T.M. Swager, J. Am. Chem. Soc. 117 (1995) 7017.
[6] R.Y. Tu, B.H. Liu, Z.Y. Wang, D.M. Gao, F. Wang, Q.L. Fang, Z.P. Zhang, Anal. Chem. 80 (2008) 3458.
[7] E.S. Forzani, D. Lu, M.J. Leright, A.D. Aguilar, F. Tsow, R.A. Iglesias, Q. Zhang, J. Lu, J.H. Li, N.J. Tao, J. Am. Chem. Soc. 131 (2009) 1390.
[8] Y. Mizuta, T. Onodera, P. Singh, K. Matsumoto, N. Miura, K. Toko, Biosens. Bioelectron. 24 (2008) 191.
[9] J.S. Yang, T.M. Swager, J. Am. Chem. Soc. 120 (1998) 11864.
[10] M.S. Meaney, V.L. McGuffin, Anal. Bioanal. Chem. 391 (2008) 2557.
[11] D.M. Gao, Z.Y. Wang, B.H. Liu, L. Ni, M.H. Wu, Z.P. Zhang, Anal. Chem. 80 (2008) 8545.
[12] W.C.W. Chan, S.M. Nie, Science 281 (1998) 2016.
[13] W.U. Huynh, J.J. Dittmer, A.P. Alivisatos, Science 295 (2002) 2425.
[14] V.I. Klimov, A.A. Mikhailovsky, S. Xu, A. Malko, J.A. Hollingsworth, C.A. Leatherdale, H.-J. Eisler, M.G. Bawendi, Science 290 (2000) 314.
[15] S. Coe, W.-K. Woo, M.G. Bawendi, V. Bulovic, Nature 420 (2002) 800.
[16] W.W. Zhong, Anal. Bioanal. Chem. 394 (2009) 47.
[17] W.C.W. Chan, D.J. Maxwell, X.H. Gao, R.E. Bailey, M.Y. Han, S.M. Nie, Curr. Opin. Biotechnol. 13 (2002) 40.
[18] J.M. Klostranec, W.C.W. Chan, Adv. Mater. 18 (2006) 1953.
[19] X. Michalet, F.F. Pinaud, L.A. Bentolila, J.M. Tsay, S. Doose, J.J. Li, G. Sundaresan, A.M. Wu, S.S. Gambhir, S. Weiss, Science 307 (2005) 538.
[20] A.P. Alivisatos, Nat. Biotechnol. 22 (2004) 47.
[21] J.K. Jaiswal, S.M. Simon, Trends. Cell. Biol. 14 (2004) 497.
[22] I.L. Medintz, H.T. Uyeda, E.R. Goldman, H. Mattoussi, Nat. Mater. 4 (2005) 435.
[23] W.J. Jin, M.T. Fernandez-Arguelles, J.M. Costa-Fernandez, R. Pereiro, A. Sanz-Medel, Chem. Commun. (2005) 883.
[24] J.M. Costa-Fernández, R. Pereiro, A. Sanz-Medel, Trends. Anal. Chem. 25 (2006) 207.

[25] K.S. Novoselov, A.K. Geim, S.V. Morozov, D. Jiang, Y. Zhang, S.V. Dubonos, I.V. Grigorieva, A.A. Firsov, Science 306 (2004) 666.
[26] A.K. Geim, K.S. Novoselov, Nat. Mater. 6 (2007) 183.
[27] X.L. Li, X.R. Wang, L. Zhang, S.W. Lee, H.J. Dai, Science 319 (2008) 1229.
[28] D.V. Kosynkin, A.L. Higginbotham, A. Sinitskii, J.R. Lomeda, A. Dimiev, B.K. Price, J.M. Tour, Nature 458 (2009) 872.
[29] L.A. Ponomarenko, F. Schedin, M.I. Katsnelson, R. Yang, E.W. Hill, K.S. Novoselov, A.K. Geim, Science 320 (2008) 356.
[30] M.M. Müller, X. Yan, J.A. McGuire, L.-S. Li, Nano Lett. 10 (2010) 2679.
[31] X. Yan, B. Cui, L.-S. Li, J. Am. Chem. Soc. 132 (2010) 5944.
[32] D.Y. Pan, J.C. Zhang, Z. Li, M.H. Wu, Adv. Mater. 22 (2010) 734.
[33] S.J. Zhu, J.H. Zhang, C.Y. Qiao, S.J. Tang, Y.F. Li, W.J. Yuan, B. Li, L. Tian, F. Liu, R. Hu, H.N. Gao, H.T. Wei, H. Zhang, H.C. Sun, B. Yang, Chem. Commun. 47 (2011) 6858.
[34] V. Gupta, N. Chaudhary, R. Srivastava, G.D. Sharma, R. Bhardwaj, S. Chand, J. Am. Chem. Soc. 133 (2011) 9960.
[35] Y. Li, Y. Hu, Y. Zhao, G.Q. Shi, L.E. Deng, Y.B. Hou, L.T. Qu, Adv. Mater. 23 (2011) 776.
[36] J.H. Shen, Y.H. Zhu, C. Chen, X.L. Yang, C.Z. Li, Chem. Commun. 47 (2011) 2580.
[37] S. Empedocles, M. Bawendi, Acc. Chem. Res. 32 (1999) 389.
[38] M.A. El-Sayed, Acc. Chem. Res. 37 (2004) 326.
[39] H. Zhang, J. Han, B. Yang, Adv. Funct. Mater. 20 (2010) 1533.
[40] W.S. Hummers, R.E. Offeman, J. Am. Chem. Soc. 80 (1958) 1339.
[41] L.S. Fan, Q.X. Zhang, K.K. Wang, F.H. Li, L. Niu, J. Mater. Chem. 22 (2012) 6165.
[42] A. Ambrosi, A. Bonanni, Z. Sofer, J.S. Cross, M. Pumera, Chem. Eur. J 17 (2011) 10763.
[43] X. Li, X. Wang, L. Zhang, S. Lee, H. Dai, Science 319 (2008) 1229.
[44] V.C. Tung, M.J. Allen, Y. Yang, R.B. Kaner, Nat. Nanotechnol 4 (2009) 25.
[45] C. Zhu, S. Guo, Y. Fang, S. Dong, ACS Nano 4 (2010) 2429.
[46] L.R. Radovic, B. Bockrath, J. Am. Chem. Soc. 127 (2005) 5917.
[47] S. Kochmann, T. Hirsch, O.S. Wolfbeis, J. Fluoresc. (2011), http://dx.doi.org/10.1007/s10895-011-1019-8.
[48] M. Sykora, M.A. Petruska, J. Alstrum-Acevedo, I. Bezel, T.J. Meyer, V.I. Klimov, J. Am. Chem. Soc. 128 (2006) 9984.
[49] A. Cao, Z. Liu, S. Chu, M. Wu, Z. Ye, Z. Cai, Y. Chang, S. Wang, Q. Gong, Y. Liu, Adv. Mater. 22 (2010) 103.
[50] J.R. Lakowicz, Principles of Fluorescence Spectroscopy, Kluwer Academic/Plenum Press, New York, 1999.